A high-precision study of polarized proton scattering to low-lying states in 11B

Hannen, Volker Michael

Publication date:
2001

Link to publication in University of Groningen/UMCG research database

Citation for published version (APA):
Hannen, V. M. (2001). *A high-precision study of polarized proton scattering to low-lying states in 11B*. s.n.

4. Determination of cross sections and analyzing powers

The main objective of the $^{11}\text{B}(\vec{p}, p')^{11}\text{B}$ experiment was to measure differential cross sections and analyzing powers of low-lying states in ^{11}B in order to extract electromagnetic transition strengths. The measurements have been performed using 150 MeV polarized protons (for the values of the beam polarization during the measurements see table 3.1). Data were taken at a number of spectrometer angles between 5° and 28° alternately on a 20.1 mg/cm^2 thick self-supporting ^{11}B target with an enrichment of 99.5% [93] and on a 9.0 mg/cm^2 thick natural carbon target. Data from the ^{12}C measurements are used to cross check our experimental results against measurements from groups at other laboratories [94, 95, 96, 97] and, therefore, provide a possibility to verify the correct functioning of the detector systems and of the analysis procedure applied in this work. Although no information from the FPP is required for the determination of cross sections and analyzing powers, the polarimeter was running during most of the measurements and the analysis of the additional data is described in chapter 5. The following sections describe the procedures involved in the extraction of angular distributions of cross sections and analyzing powers from the experimental data. If possible, results of the analysis will be compared with existing data from the literature in section 4.4.

4.1 Kinetic energy and solid angle

The kinetic energy E of charged particles analyzed in the BBS can be obtained from their magnetic rigidity $B\rho$ via [98]

$$B\rho = \frac{3.3356}{q} \sqrt{2m_0c^2E + E^2} \ \text{kG} \cdot \text{cm} , \tag{4.1}$$

where q is the charge state and E and m_0c^2, the rest-energy of the particle, are given in MeV. Using a fit function as described in section 3.4.2, the target coordinates δ, ϑ_t and φ_t are calculated from the focal-plane coordinates of the particle. The angles ϑ_t and φ_t are the horizontal and vertical scattering angles of the particle relative to the central ray of the BBS and δ is the
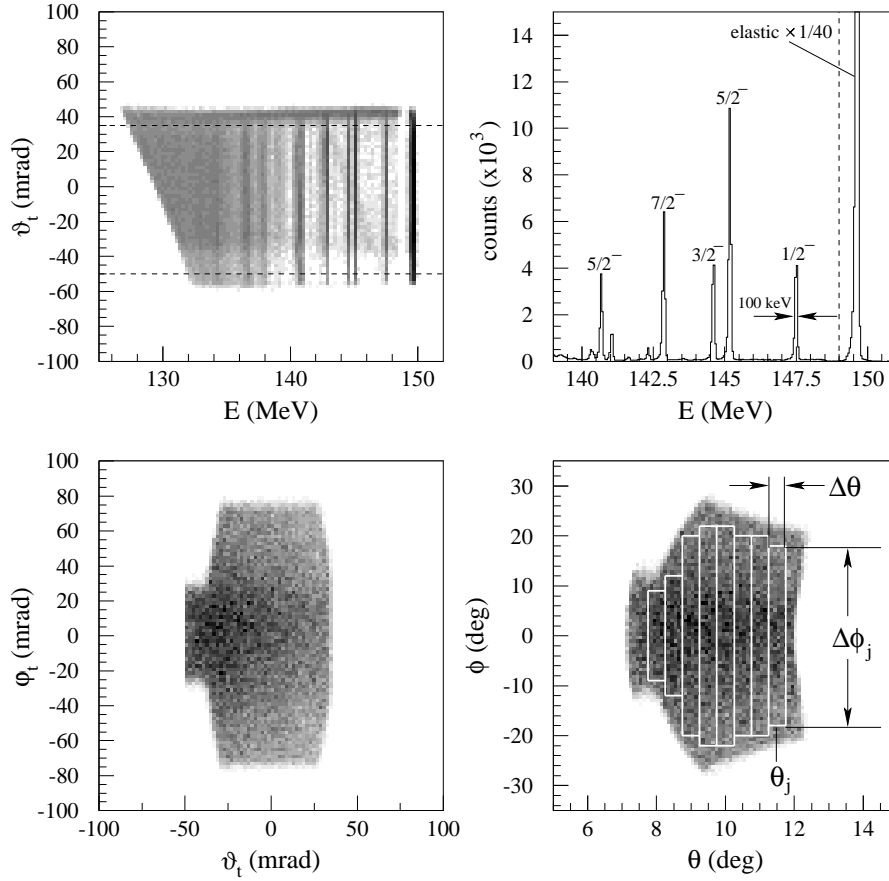
Figure 4.1: Plots produced from a measurement in which 150 MeV protons have been scattered from ^{11}B at a spectrometer angle $\Theta_{BBS} = 10°$. The states observed in the upper right panel have been identified using reference [11].

---

relative magnetic rigidity $\delta = (B\rho - B\rho_0)/(B\rho_0)$, with $B\rho_0$ being the rigidity of the central ray. Inserting δ into equation 4.1 and solving for E then results in

$$E = -m_0 c^2 + \sqrt{m_0^2 c^4 + \left(\frac{B\rho_0(\delta + 1)}{\text{kG} \cdot \text{cm}} \frac{q}{3.3356}\right)^2}. \qquad (4.2)$$

The upper left panel in figure 4.1 shows the horizontal angle ϑ_t plotted against the resulting kinetic energy for 150 MeV protons scattered from ^{11}B at a spectrometer angle $\Theta_{BBS} = 10°$. Vertical lines observed in the plot correspond to states in ^{11}B with the ground state at the highest energy.
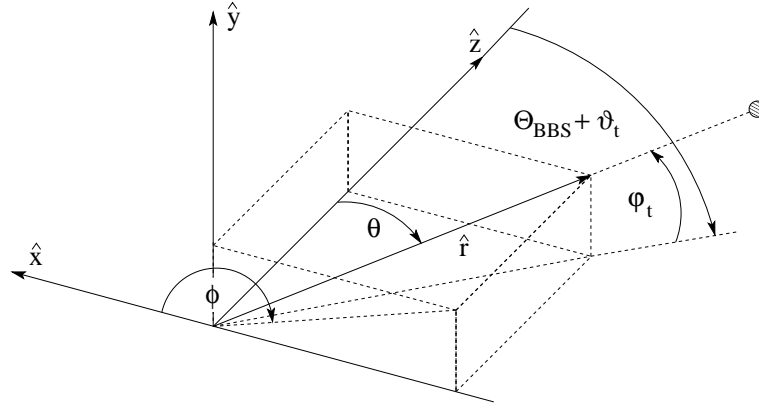
Figure 4.2: Relation of the target coordinates ϑ_t and φ_t to the spherical angles θ and ϕ for a particular outgoing particle track.

Events outside the area enclosed between the horizontal dashed lines are rejected to reduce instrumental background. The energy spectrum of the scattered protons is shown in the upper right panel of figure 4.1. The elastic-scattering line, which at this angle is located at an energy of 149.55 MeV, has been scaled down by a factor 40. The FWHM of the peak located at $E = 147.43$ MeV, which corresponds to the $J^{\pi} = 1/2^-$ state, is about 100 keV.

By plotting the vertical target angle φ_t versus the horizontal angle ϑ_t one obtains an image of the opening of the spectrometer (see figure 4.1, lower left). For the determination of the solid angle, however, these angles have to be converted into spherical coordinates. Figure 4.2 shows the relation of the target angles ϑ_t and φ_t of a certain particle track to the polar scattering angle θ and the azimuthal angle ϕ. The direction $\hat{r}$ of the outgoing particle is given by

$$\hat{r} = \begin{pmatrix} \sin(\Theta_{BBS} + \vartheta_t) \cdot \cos\varphi_t \\ \sin\varphi_t \\ \cos(\Theta_{BBS} + \vartheta_t) \cdot \cos\varphi_t \end{pmatrix} . \tag{4.3}$$

From this the polar angle θ can be calculated by the scalar product between $\hat{z} = (0,\ 0,\ 1)$ and $\hat{r}$ to be

$$\theta = \arccos(\hat{z} \cdot \hat{r}) = \arccos[\cos(\Theta_{BBS} + \vartheta_t) \cdot \cos\varphi_t] , \tag{4.4}$$

while the azimuthal angle is given by $\phi = \arctan(r_y/r_x)$, which results in

$$\phi = \arctan\left(\frac{\tan\varphi_t}{\sin(\Theta_{BBS} + \vartheta_t)}\right) \ . \tag{4.5}$$

When plotting the azimuthal versus the polar angle, one obtains a spherical representation of the BBS opening as shown in the lower right panel of figure 4.1. In this representation the angular acceptance of the spectrometer can easily be divided into strips with a well defined scattering angle θ_j and solid angle $\Delta\Omega_j = \sin\theta_j\Delta\theta\Delta\phi_j$, as is indicated in the figure.

4.2   Polarized-beam cross section

To extract cross sections from the accumulated data, the counts collected inside a certain solid angle bin $\Delta\Omega_j$ and energy bin ΔE_i have to be corrected for the measured dead-times of the setup, for the reconstruction efficiency of the VDCs and for the integrated charge. In case of a polarized-beam measurement this has to happen separately for each of the polarization states of the beam. The corrected number of counts per unit charge $C_{\kappa ij}$, for a certain polarization state κ inside the ith energy bin and the jth solid-angle strip, then becomes

$$C_{\kappa ij} = \frac{N_{\kappa ij}}{(1 - D_\kappa)Q_\kappa \Upsilon} \ , \tag{4.6}$$

with

$$
\begin{aligned}
N_{\kappa ij} &= \text{uncorrected counts,} \\
D_\kappa &= \text{dead-time,} \\
Q_\kappa &= \text{integrated charge (in [nC], see equation 4.9),} \\
\Upsilon &= \text{VDC efficiency (see section 3.5.1).}
\end{aligned}
$$

The integrated charge Q_κ is monitored using a Faraday cup installed in the beam stop, while the dead-time D_κ can be calculated from the ratio of triggers to the number of acquired events (see section 3.6.3).

A problem that surfaced during data analysis is that the hit density for a fixed scattering angle θ_j decreases when going from the central region of the BBS opening to the upper or lower edge of the acceptance. Quantitatively, the hit density in the central region of the angular acceptance differed by up to 15% from the overall density observed inside a solid-angle strip belonging to a certain scattering angle θ_j.

The variation of the cross section due to the analyzing power of a particular

nuclear reaction is, for a proton beam of polarization $\vec{p}_\kappa = (0, p_y^\kappa, 0)$, given by

$$\left.\frac{d\sigma}{d\Omega}(\theta_j, \phi)\right|_\kappa = \left.\frac{d\sigma}{d\Omega}(\theta_j)\right|_0 \left(1 + p_y^\kappa \cos \phi A_n(\theta_j)\right) , \text{ with} \qquad (4.7)$$

$$\left.\frac{d\sigma}{d\Omega}(\theta_j)\right|_0 = \text{cross section for an unpolarized beam .}$$

The resulting variation in the hit density at a spectrometer angle $\Theta_{BBS} = 5°$ can be estimated, assuming values $p_y = 0.7$, $A_n(5°) = 0.36$ (corresponding to the analyzing power of elastic scattering from ^{12}C, see figure 4.4, right panel) and an azimuthal coverage of $|\phi| \leq 40°$, to be about 4%. At larger spectrometer angles the effect due to the analyzing power becomes smaller because of the decreasing azimuthal coverage of the BBS. For instance, at $\Theta_{BBS} = 21°$, where the analyzing power of the elastic scattering reaches its maximum value of $A_n \approx 0.9$ and $|\phi| \leq 11°$, the effect is only about 2%. The experimentally observed variations can, therefore, not be explained by the reaction mechanism, but must have an, at the time of this writing, unknown instrumental origin.

To correct for the effect, an additional factor ξ_j has been introduced, defined by the ratio of the central to the overall hit density inside a certain solid angle strip, such that the corrected number of counts per unit charge becomes

$$C_{\kappa ij} = \frac{N_{\kappa ij}\xi_j}{(1 - D_\kappa)Q_\kappa \Upsilon} . \qquad (4.8)$$

Because the factor ξ_j is averaged between the spin-up and spin-down phases of the beam polarization, which have roughly the same magnitude $|p_y|$ but opposite signs, it is ensured that only the instrumental effect is corrected for and not the real physical variation due to the analyzing power $A_n(\theta)$.

The double-differential cross section for a proton beam of polarization $\vec{p}_\kappa$ is then given by

$$\left.\frac{d^2\sigma}{d\Omega dE}(E_i, \theta_j)\right|_\kappa = 0.266 \cdot 10^{-3} \cdot \frac{A}{\mu} \frac{C_{\kappa ij}}{\Delta\Omega_j \Delta E_i} \left[\frac{\text{mb}}{\text{sr MeV}}\right] , \qquad (4.9)$$

with

$$\begin{aligned} A &= \text{target mass [g/mol],} \\ \mu &= \text{target thickness [g/cm}^2\text{],} \\ \Delta\Omega_j &= \text{solid angle [sr],} \\ \Delta E_i &= \text{energy bin [MeV].} \end{aligned}$$
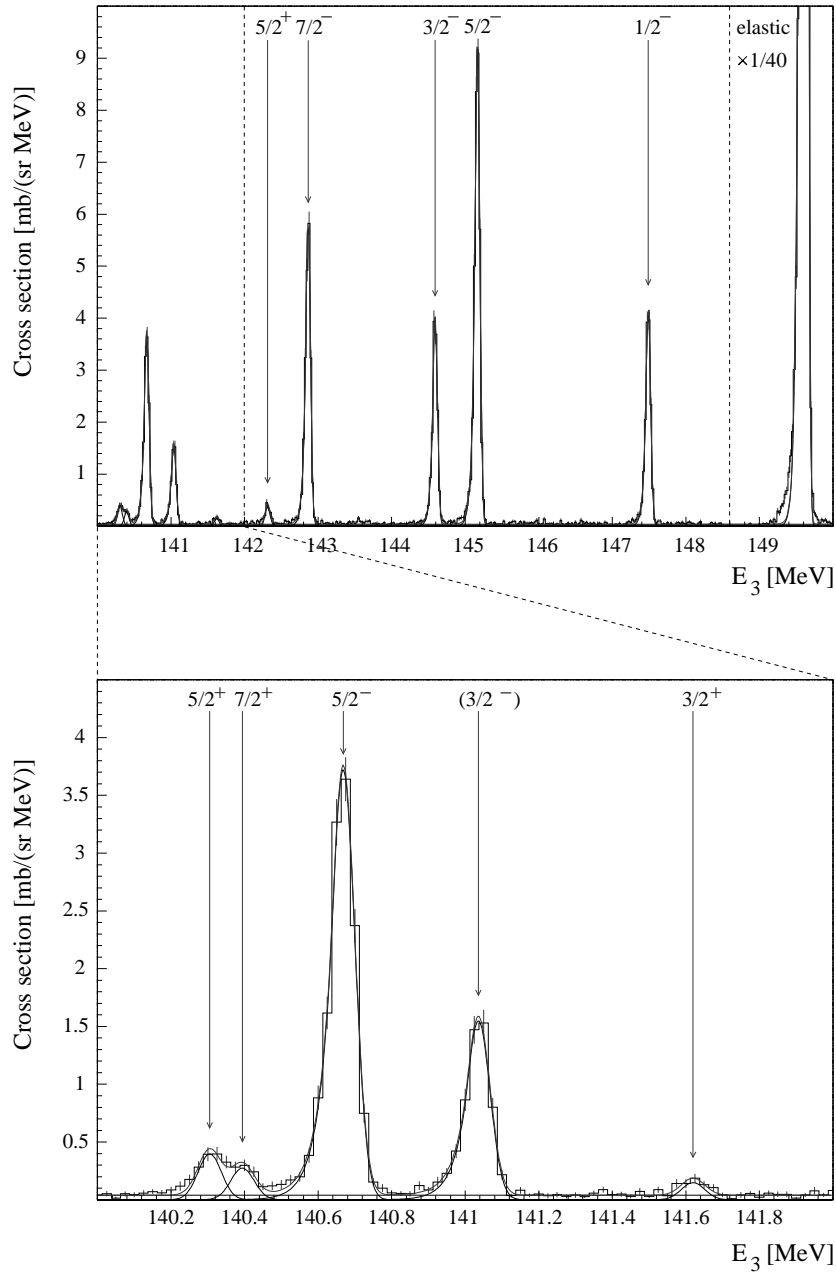
Figure 4.3: Double-differential cross section of the reaction $^{11}\text{B}(\vec{p}, p')^{11}\text{B}$ at $\Theta_{BBS} = 10°$ as a function of the kinetic energy of the ejectiles. The spin assignments of the states have been taken from reference [11].

Figure 4.3 shows the kinetic-energy spectrum of the double-differential cross section for 150 MeV polarized protons scattered from ^{11}B at $\Theta_{BBS} = 10°$. To extract angular distributions of cross sections and analyzing powers of the observed states, the energy spectra at each angle θ_j and polarization $\vec{p}_\kappa$ are fitted using the code FIT [99]. The line shape is approximated by a gaussian with an exponential tail towards lower energies. The area under the nth peak in a spectrum corresponds to the differential cross section of a certain excited state at the scattering angle and beam polarization at which the spectrum was taken and will be referred to by $\left.\frac{d\sigma}{d\Omega}(\theta_j)\right|_\kappa^n$.

4.3 Analyzing power and unpolarized-beam cross section

The analyzing power $A_n(\theta)$ of a particular nuclear reaction can be determined by performing measurements with different beam polarizations p_y^1 and p_y^2. Dividing the cross sections given by equation 4.7 for the two polarization states one obtains

$$\frac{\left.\frac{d\sigma}{d\Omega}(\theta_j, \phi)\right|_1^n}{\left.\frac{d\sigma}{d\Omega}(\theta_j, \phi)\right|_2^n} = \frac{1 + p_y^1 \cos\phi A_n(\theta_j)}{1 + p_y^2 \cos\phi A_n(\theta_j)} \tag{4.10}$$

which, when averaging over the azimuthal interval $\Delta\phi_j$, results in

$$\frac{\left.\frac{d\sigma}{d\Omega}(\theta_j)\right|_1^n}{\left.\frac{d\sigma}{d\Omega}(\theta_j)\right|_2^n} = \frac{1 + p_y^1 \Pi_j A_n(\theta_j)}{1 + p_y^2 \Pi_j A_n(\theta_j)} \ , \tag{4.11}$$

with

$$\Pi_j = \frac{1}{\Delta\phi_j} \int_{\Delta\phi_j} \cos\phi \, d\phi \ . \tag{4.12}$$

Solving equation 4.11 for $A_n(\theta_j)$ one gets

$$A_n(\theta_j) = \frac{\left.\frac{d\sigma}{d\Omega}(\theta_j)\right|_1^n - \left.\frac{d\sigma}{d\Omega}(\theta_j)\right|_2^n}{\left.\frac{d\sigma}{d\Omega}(\theta_j)\right|_2^n p_y^1 \Pi_j - \left.\frac{d\sigma}{d\Omega}(\theta_j)\right|_1^n p_y^2 \Pi_j} \ . \tag{4.13}$$

Once the analyzing power of a particular reaction is known, the unpolarized-beam cross section of that reaction can be calculated from any of the polarized-beam cross sections via

$$\left.\frac{d\sigma}{d\Omega}(\theta_j)\right|_0^n = \frac{\left.\frac{d\sigma}{d\Omega}(\theta_j)\right|_\kappa^n}{1 + p_y^\kappa \Pi_j A_n(\theta_j)} \ . \tag{4.14}$$

4.4   Experimental results and comparison with existing data

Angular distributions of cross sections and analyzing powers with center-of-mass angles in the range of $4° \leq \theta_{cm} \leq 31°$ in the ^{11}B case and $4° \leq \theta_{cm} \leq 29°$ in the ^{12}C case have been extracted from the data. For ^{11}B, all positive and negative parity states up to the $J^\pi = 5/2^+$ state at an excitation energy of $E_x = 9.274$ MeV have been analyzed with the exception of the $1/2^+$ state at 6.792 MeV, which lies too close to the much stronger $7/2^-$ state at 6.743 MeV to be resolved. In case of the negative parity states the BBS acceptance has been divided into four $1°$ bins, while for the weaker positive parity states the angular bins of a setting were joined to form one $4°$ bin in order to gain sufficiently high statistics. The overall systematic uncertainty of the measured cross sections, that accounts for errors in dead-time corrections, in the calculation of inefficiencies and acceptances and in the integrated charges and target thicknesses, is assumed to be about 10%.

A comparison of elastic cross-section and analyzing-power data extracted from the ^{12}C measurements to existing data-sets measured at Orsay [95] and at IUCF [97] is shown in figure 4.4. While there is excellent agreement
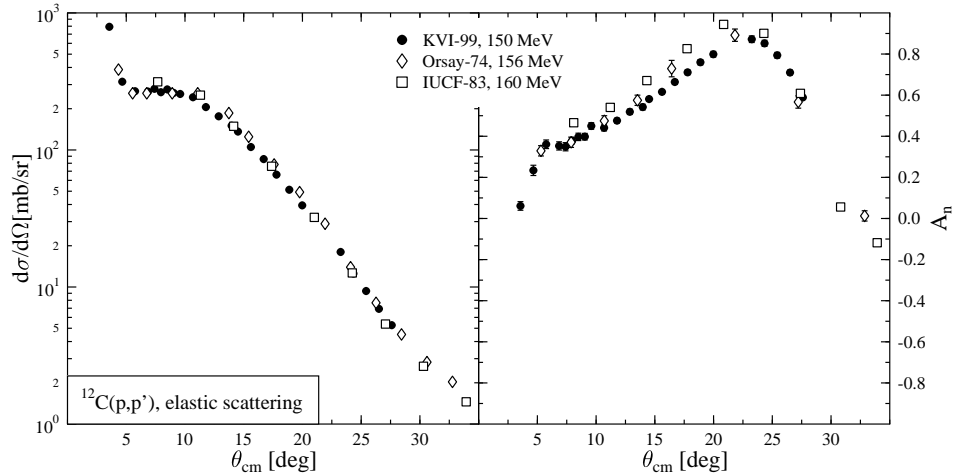

Figure 4.4: Cross section (left) and analyzing power (right) for elastic scattering of protons from ^{12}C. The Orsay-74 and IUCF-83 data-sets have been taken from references [95] and [97], respectively.
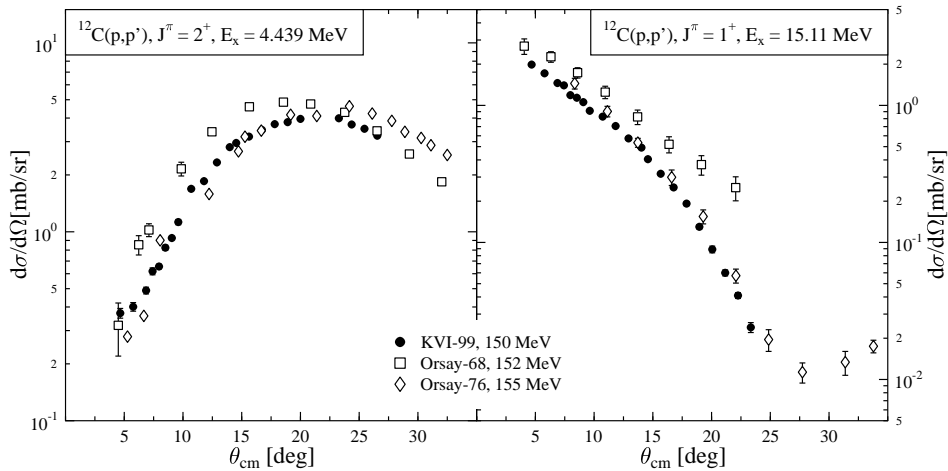
Figure 4.5: Cross sections for inelastic scattering of protons from ^{12}C to the $J^\pi = 2^+$ state at $E_x = 4.439$ MeV (left) and the $J^\pi = 1^+$ state at $E_x = 15.11$ MeV (right). The Orsay-68 and Orsay-76 data-sets have been taken from references [94] and [96], respectively.

between the cross sections observed at the different laboratories, the analyzing power measured at IUCF at an incoming proton energy of 160 MeV lies slightly above the data measured at 156 and 150 MeV at Orsay and KVI, respectively. This can be explained by the energy dependence of the elastic-scattering analyzing power in this angular region which reaches its maximum at about 200 MeV [100]. Figure 4.5 shows two examples for cross sections of inelastic transitions in ^{12}C. Data taken at KVI are compared to data-sets measured in Orsay, one in the late sixties [94] and one in the mid seventies [96]. While there is good agreement between the KVI data and the latter measurement, the older Orsay data predict a substantially higher cross section.

Figure 4.6 shows the results obtained for elastic scattering on ^{11}B compared to the only other available elastic-scattering data-set in this energy region, which has been measured at Orsay [101]. There is good agreement between the analyzing powers of the measurements, while the cross sections at smaller angles differ substantially.

For the inelastic transitions there are two more data-sets at an incoming proton energy of 185 MeV, both measured in Uppsala [102, 103], which can be used to compare with our data. Figure 4.7 shows measured cross sections
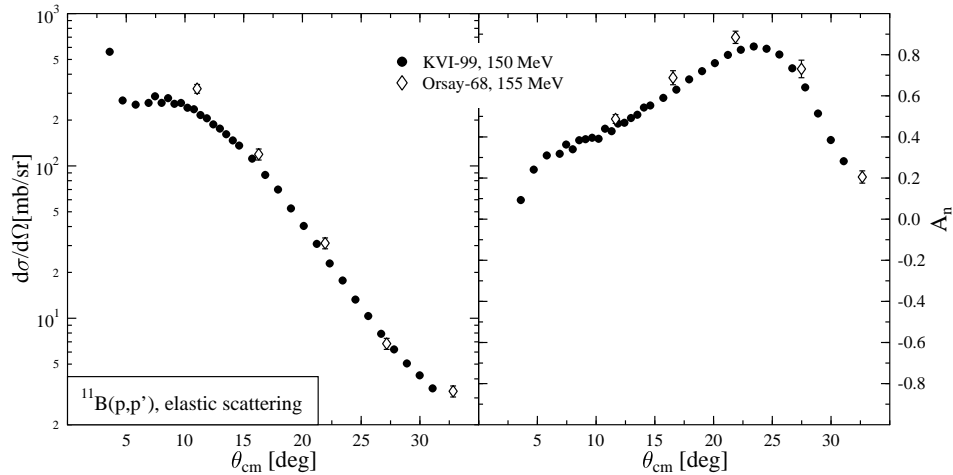
Figure 4.6: Cross section (left) and analyzing power (right) for elastic scattering of protons from ^{11}B. The Orsay-68 data-set has been taken from reference [101].

for a number of negative parity states in ^{11}B as a function of the transfered momentum q. This representation allows for an easier comparison of data-sets at different incoming proton energies. While there is agreement between the KVI data and the Uppsala measurements for some of the states and angles, the older measurements generally yield higher cross sections for the analyzed states. Two experimental circumstances may play a role in this respect. Firstly, the older measurements suffered from a poor energy resolution, which has been 350 to 450 keV in the Uppsala case and 700 to 800 keV during the Orsay experiments. This makes it difficult to separate some of the states, for instance, in the case of the $5/2^-$ state at 8.920 MeV and the two nearby positive parity states at 9.185 and 9.274 MeV which are observed as one peak. Secondly, in contrast to the KVI experiment where a self-supporting boron target was used, the older measurements were performed using pressed powder targets enclosed between aluminum or mylar foils. Protons scattered from the additional material cause an instrumental background in the energy spectra, which may not always be easy to separate from the relevant excited states in ^{11}B.
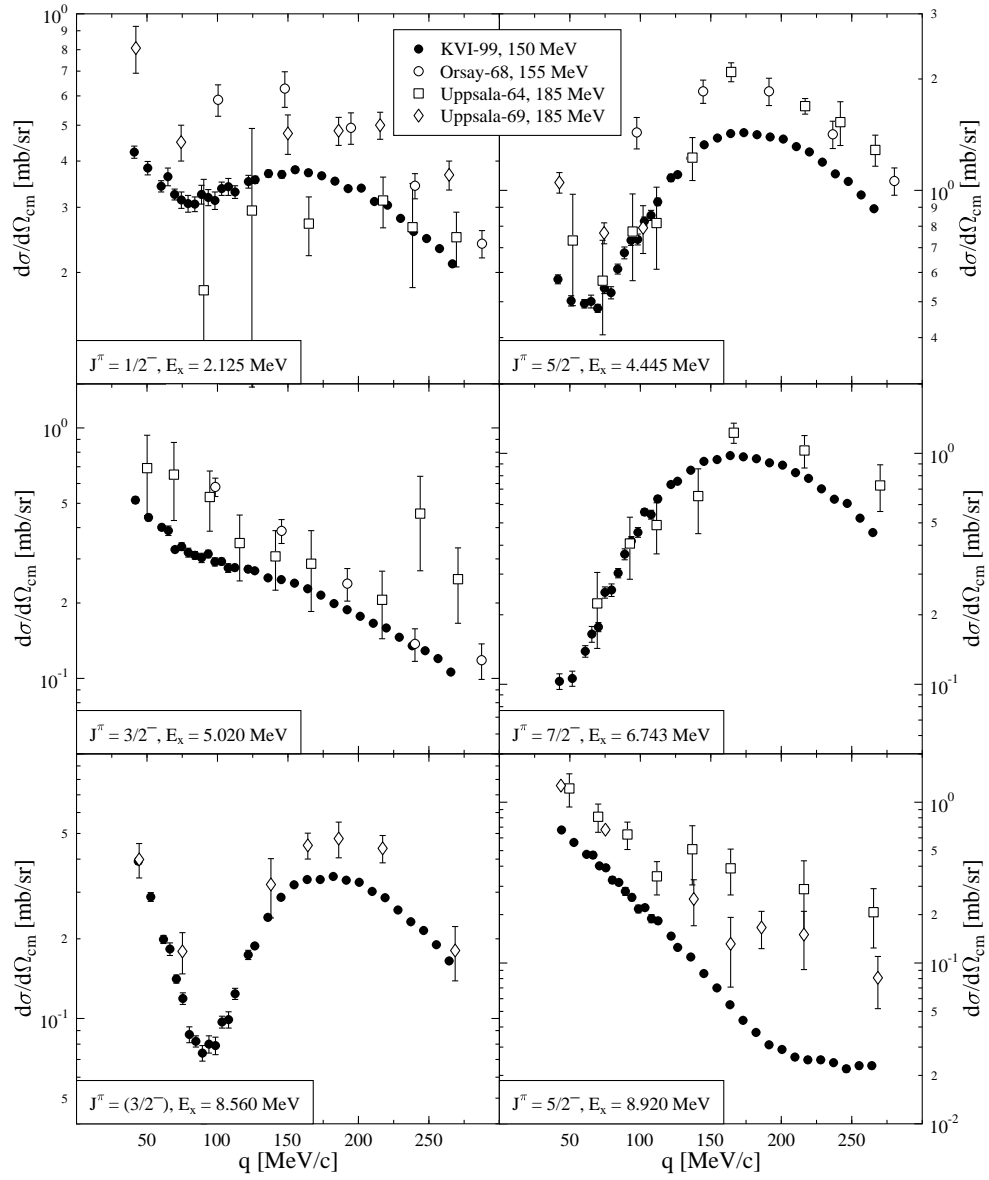
Figure 4.7: Cross sections for inelastic scattering of protons from ^{11}B to several low-lying states. The Orsay-68, Uppsala-64 and Uppsala-69 data-sets have been taken from references [101], [102] and [103], respectively. Excitation energies and spin assignments have been taken from reference [11].